Evaluation of low-cost MEMS accelerometers for measurements of velocity of unmanned vehicles

Przemysław Dąbek

Industrial Research Institute for Automation and Measurements PIAP

Abstract: Aim of the paper is to assess uncertainty associated with determination of velocity using MEMS accelerometer. Two MEMS accelerometers are evaluated from the point of view of measurement characterized by short duration and possibility of repetitions in unchanged environment. Mathematical model of measurement of velocity is presented with its accompanying uncertainty. The accelerometers were first subjected to calibration and testing of nonlinearity of their scale factors, then fixed to a wheeled robot which performed repeated manoeuvres of straight line movement on laboratory ground. Standard uncertainty of velocity measured using the examined accelerometers was at the level of 0.02–0.04 m/s for run duration of about 1.5 s and averaged data from 12 runs. MEMS accelerometers can be recommended for velocity measurements characterised by short duration and possibility of repetitions, if uncertainties of calibration and of measurement of vehicle tilt angle during motion are minimized.

Keywords: MEMS accelerometers, velocity measurement, measurement uncertainty, vehicle dynamics, unmanned vehicles

1. Introduction

Information about parameters of motion of a vehicle can be used in the industry in several ways to enhance capabilities of a product. For instance, in the mobile robotics domain, availability of motion parameters during wheeled vehicle operation enables on-line determination of the wheel-terrain friction coefficient [1], which information can be subsequently used in control algorithms to increase robot's mobility in difficult terrain, to optimize energy consumption or to improve robot's autonomous behaviour.

On the other hand, a high quality knowledge of vehicle dynamics in typical terrains of operation is essential to "calibrate" tools which aid computer design of vehicles. The mentioned tools are computer software developed around the concept of Virtual Prototyping (VP). In order for the VP technology to work, there must be available mathematical models of all necessary components of the designed system. There are persistent needs to develop models which comply with emerging applications like, for instance, small-size and lightweight unmanned ground vehicles (UGVs). An example of model of dynamics of such a vehicle (mobile robot) can be found in [2].

One of techniques of measurement of motion parameters is inertial measurement of acceleration, which can be then subjected to integration to yield velocity or position.

An instrument for inertial measurement of motion parameters is called the Inertial Measurement Unit (IMU) and usually contains 3 accelerometers and 3 gyroscopes, which permit a 6-degrees-of-freedom measurement.

Accelerometers and gyroscopes used in the IMU can be manufactured in the micro-electro-mechanical-systems technology (MEMS). Advantages of the MEMS accelerometers over electromechanical sensors include smaller dimensions, lower weight and most importantly lower price. On the other hand, MEMS accelerometers tend to have worse performance, that is, higher scale factor error and lower resolution.

Despite strong advantages, sometimes MEMS accelerometers are not even considered by an engineering team as potential solution for measurements of velocity or position, because of prevailing view that their performance is inferior. Although in some cases opinions like that may be justified, one should be aware of development rapidly going on in the MEMS field. Recently was published the analysis which forecasts dramatic growth of the MEMS market – 25-fold increase in sales in 2025 as compared to 2005 [3]. Also in work [4] improvements in MEMS IMU precision and decrease of price are foreseen before 2020. For those reasons, it is author's strong belief, that the market of MEMS accelerometers should be monitored for improvements and their performance evaluated from the point of view of application to measurement of velocity or position.

An extensive account of previous work done in the field of inertial measurement can be found in work [5]. Also in the work [5] findings related to inertial measurement of distance using a MEMS accelerometer are presented. Recently there are successful attempts to remove gyroscopes from the design of MEMS IMU and use only accelerometers for measurements of angular velocity [6].

The objective of this article is to find out the uncertainty of measurement of vehicle translational velocity by means of recently produced budget MEMS acceleration sensors.

This knowledge will inform decision if the low-cost accelerometers are suitable for the task of gathering data necessary to validate non-linear dynamics model of the kind described in work [2]. Velocity is the crucial motion parameter in this application.

One should bear in mind, that the characterisation of motion of unmanned vehicle for the purpose of validation of its dynamics model usually has the following properties:

1) it does not require long duration of measurement (typically, less than one minute),
2) the measurement can be repeated in laboratory conditions.

2. Examined MEMS accelerometers

There is a variety of MEMS instruments for acceleration measurement available on the market today, which may be all termed with a common name of "accelerometers". In fig. 1 an accelerometer is modelled as a stack of three functional layers: (1) mechanical layer responsible for acceleration sensing, structural support and protection, (2) electronic layer to convert displacement of mechanical sensing element into electrical signal, (3) interface layer to encode analogue electrical signal according to the protocol rules to enable connection to one of standardized buses, e.g. USB. In this article instruments which consist of layers 1 and 2 will be referred to as *transducers*, whereas of layers 1, 2 and 3, as *measurement system nodes*.

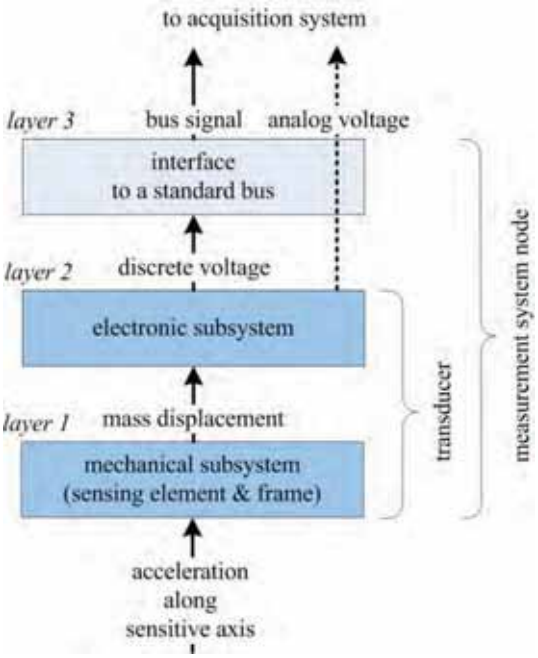

Fig. 1. Layered model of a MEMS accelerometer: layer 1 is a sensor, layers 1 and 2 constitute a transducer, layers 1, 2, 3 – a measurement system node

Rys. 1. Model warstwowy akcelerometru typu MEMS: warstwa 1 – czujnik, warstwy 1 i 2 to przetwornik, warstwy 1, 2, 3 – węzeł systemu pomiarowego

Measurement system nodes (layers 1-3) examined in the present study are shown in fig. 2. In tab. 1 their properties are compared with MEMS Inertial Measurement Unit suitable for navigation tasks (layers 1–3), and with MEMS acceleration transducer (layers 1–2).

The ADIS16375 IMU specification is provided in tab. 1, as an example of an instrument of higher grade, in order to highlight lower performance parameters of the measurement nodes considered in the present study. The acceleration sensor ADXL330 can be considered as a basic component of the examined accelerometers. Although suppliers do not provide information about the transducers used, in case of the Phidget accelerometer, the transducer has been identified after examination of elements on the printed circuit board.

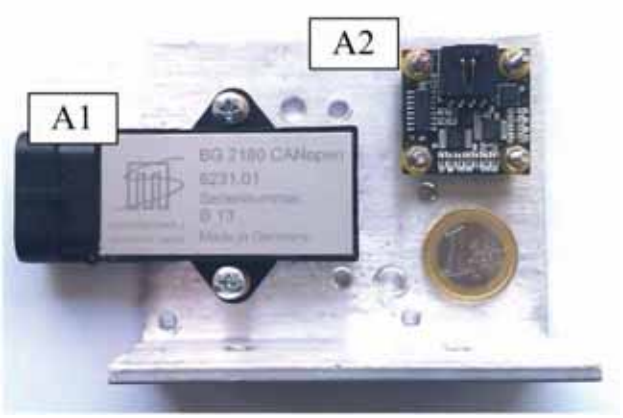

Fig. 2. Measurement nodes for acceleration measurement examined in the present study

Rys. 2. Węzły pomiarowe do pomiaru przyspieszenia badane w niniejszej pracy

Tab. 1. Properties of accelerometers A1 and A2 compared with instruments of different measurement quality

Tab. 1. Właściwości akcelerometrów A1 i A2 na tle instrumentów oferujących inną jakość pomiaru

Instrument / Property	ADIS 16375 [7]	BG 2180 [8]	Phidget 1059 [9]	ADXL 330 [10]
Alias	–	A1	A2	–
Price (EUR)	900	250	100	3
Range (g)	±18	±15	±3	±3
Bandwidth (Hz)	330	100	30	550
Nonlinearity (% FS[1)])	<0.1 (10 g)	<0.1 (1 g)	< 0.5 (1 g)	- < 0.3
Misalignment (°)	<0.035	<0.1	<0.1	<0.1
ND[2)] x ($mg/\sqrt{Hz}$)	0.06	0.30	0.28	0.28
ND y ($mg/\sqrt{Hz}$)	0.06	0.30	0.28	0.28
ND z ($mg/\sqrt{Hz}$)	0.06	0.39	0.42	0.35
Output signal	digital	digital	digital	analog
Interface	SPI[3)]	CAN[4)]	USB[5)]	n/a
PC-ready	no	no	yes	no

[1)] FS – full scale (or limit of the range as indicated), [2)] ND – noise density, [3)] SPI – serial peripheral interface, [4)] CAN – controller area network, [5)] USB – universal serial bus

Information in tab. 1 comes from products' datasheets, except for noise and nonlinearity values for the accelerometers A1 and A2, which were obtained as a result of this study. The presented bandwidths are 3 dB Bandwidths. Noise values are given individually for each sensi-

tive axis of an instrument. They are expressed in the units of noise density (ND), because of different bandwidths of the compared instruments.

As far as the output signal is concerned, analogue output is common in case of the transducers. For instruments dedicated to general embedded applications, some kind of a universal digital interface is provided, e.g. Serial Peripheral Interface. The controller area network (CAN) interface is typical in devices intended for automotive applications. The USB interface, which enables direct PC connection, can be found as standard in the Phidgets products [9]. In this case the instrument is ready to use after drivers installation.

3. Experiments and acquisition system

The main experiment, aimed at providing data to verify accelerometer capability to measure velocity of a vehicle, involved a mobile robot (fig. 3). The robot comes from the family of PIAP Scout robots [11] produced in the Industrial Research Institute for Automation and Measurements PIAP.

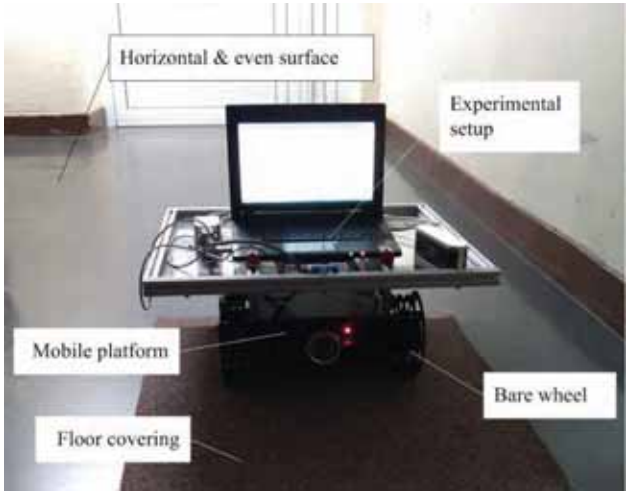

Fig. 3. Mobile platform of the Scout robot with experimental setup

Rys. 3. Platforma mobilna robota Scout z oprzyrządowaniem do prowadzenia eksperymentu

The time-course of desired linear velocity of robot wheels imposed during experiment is shown in fig. 4.

This represents a manoeuvre of straight line driving with magnitude of initial and final linear acceleration equal to about 2.0 m/s^2 and duration of 1.5 s.

The robot has been used with the following configuration: rear wheel drive, without tyres, and mass of 15.5 kg (with equipment). The ground surface was even and horizontal. Tyres were removed in order not to introduce vertical disturbances due to tyre tread of non-uniform radial length. However, a hard wheel on hard surface produced other kind of disturbances, so a piece of floor covering was used as a damping element.

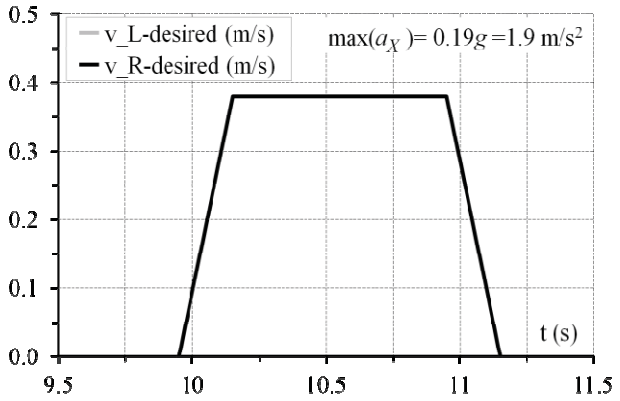

Fig. 4. Desired linear velocity profiles for left and right driven wheel of the robot

Rys. 4. Zadane profile prędkości liniowej dla lewego i prawego koła napędzanego robota

For the purpose of calibration of the accelerometers the standard 6 position static test [12] has been conducted. It requires aligning each of 3 reference axes of accelerometer with the gravity acceleration vector, both in positive and negative direction, thus giving 6 positions. In each of the 6 cases raw results from all 3 axes are recorded.

Another test was a harmonic excitation dynamic test. This test subjects an accelerometer to harmonic kinematic excitation, which has been performed using Tira-VIB vibration system (fig. 5) available in the PIAP Institute.

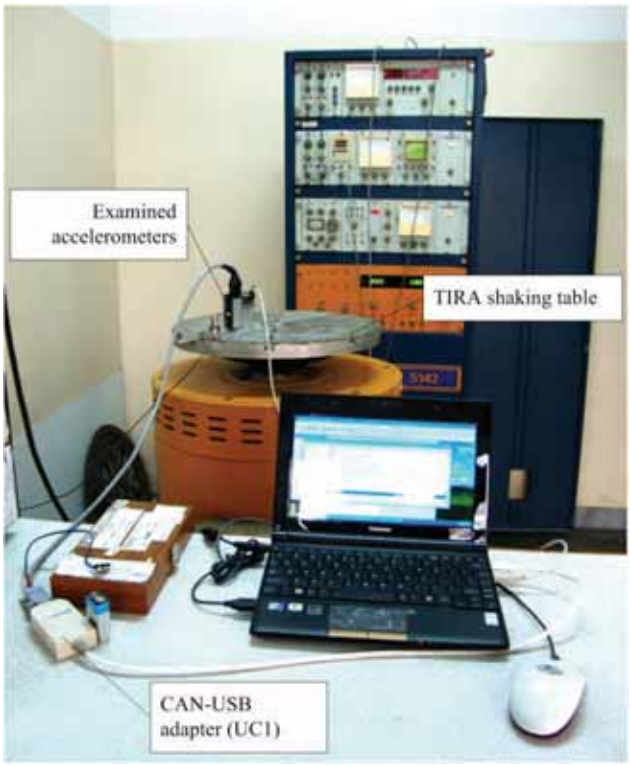

Fig. 5. Tira-VIB vibration system and setup for dynamic tests of accelerometers (PIAP)

Rys. 5. System wibracyjny Tira-VIB i oprzyrządowanie do testów dynamicznych akcelerometrów (PIAP)

The mode of operation of the Tira-VIB system, where step change in frequency generates proportional change in the amplitude of generated harmonic acceleration, has been used with frequencies 1–10 Hz. The purpose of the dynamic test was to investigate the non-linearity of the accelerometer scale factor.

The acquisition system is designed primarily to fit the limited space available on the small mobile robot. It is based on a mobile PC (mini notebook) with installed Microsoft Windows XP operating system and the dedicated application to perform tasks of a measurement system (object control plus data acquisition). Architecture of the adopted measurement system is shown in fig. 6.

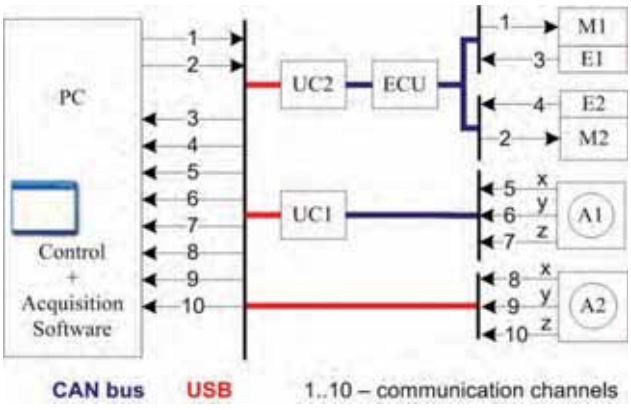

Fig. 6. Architecture of the measurement system
Rys. 6. Architektura systemu pomiarowego

The measurement system is capable of cooperation with two accelerometers (A1, A2) and two drive units of the UGV (M1, M2). Encoders of the drive units can be monitored as well (E1, E2). Access to the robot electronic control unit (ECU), which manages communication at channels 1-4 on the robot side, is provided through CAN bus. The PC is equipped with standard USB ports, therefore USB-CAN adapter (UC2) is exploited to establish the connection [13]. One of the used accelerometers provides CAN bus interface, but could not be connected to the robot bus, as there were no matching bit rate between robot ECU and A1. As a result additional USB-CAN adapter (UC1) must have been introduced to the system.

4. Model of measurement of velocity

The measurand is defined as the horizontal component of translational velocity of mass centre of a vehicle v_X. Changes of velocity v_X are primarily due to acceleration a_X generated by driving force F_X in the contact area between wheels and the ground (fig. 7).

In fig. 7 the $O_W X_W Z_W$ coordinate system is the inertial frame of reference and the Z_W axis is vertical. Coordinate systems $O_A x_A z_A$ and $O_R x_R z_R$ are rigidly connected to vehicle's body. Axes with index "A" denote reference axes of an accelerometer. They are associated with accelerometer housing and are not the same as sensitive axes of the sensor. The sensitive axes may possess slightly different directions than reference axes, because of inaccuracy of manufacturing process. Axes with index "R" refer to axes of the robot's body. It is assumed that x_R axis is horizontal if the vehicle stands on a horizontal plane. This is true in case of the robot used in the experiment.

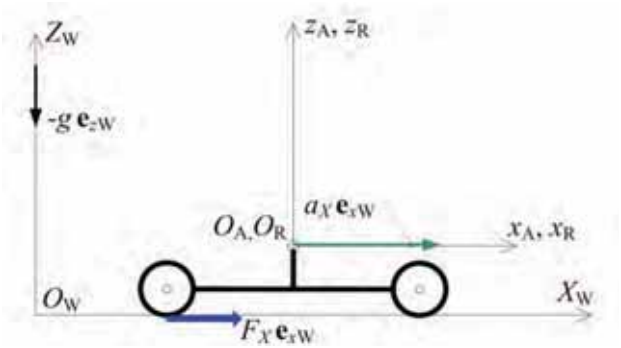

Fig. 7. Coordinate systems used in derivation of measurement model and acceleration a_X
Rys. 7. Układy współrzędnych wykorzystywane przez model pomiaru oraz przyspieszenie a_X

Fig. 8 shows the most important uncertainty sources associated with measurement of acceleration by means of a MEMS accelerometer, overlapped on the model from fig. 1. Those uncertainty sources can be divided into internal and external from the point of view of the instrument.

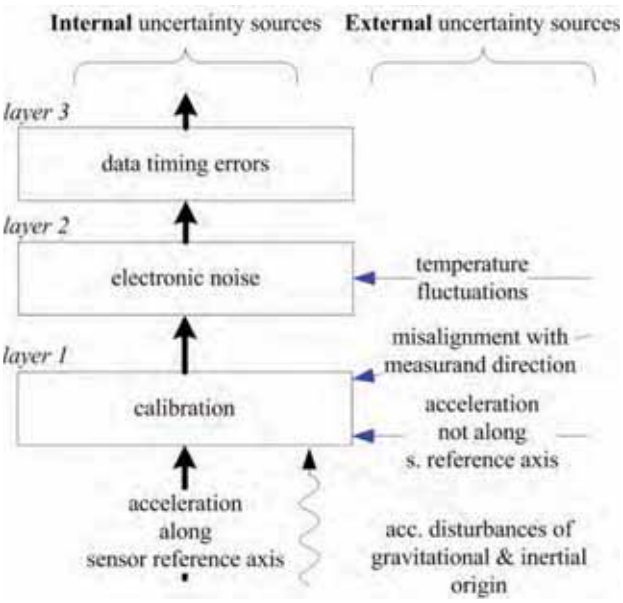

Fig. 8. The most important external and internal sources of uncertainty involved in measurement with a MEMS accelerometer
Rys. 8. Najistotniejsze zewnętrzne i wewnętrzne źródła niepewności związane z pomiarem za pomocą akcelerometru typu MEMS

The internal sources of uncertainty include: uncertainty of corrections obtained from instrument calibration, uncertainty of raw result caused by presence of electronic noise in the output signal, uncertainty of time instant at which a discrete measurement result has been captured.

According to [12] the model of measurement made with an accelerometer at any instant of time can be represented in the form

$$a_i^{\mathrm{m}} = (1+S_i)a_i^{\mathrm{t}} + m_{ij}a_j^{\mathrm{t}} + m_{ik}a_k^{\mathrm{t}} + B_i + \varepsilon_i \qquad (1)$$

where $a^{\mathrm{m}}{}_i$ is the raw result of measured acceleration along reference axis i, $a^{\mathrm{t}}{}_i$ is true acceleration, B_i is the zero bias, S_i is the scale factor error, m_{ij} (m_{ik}) is an element of the non-orthogonality matrix, and ε_i represents the random error.

The raw result $a^{\mathrm{m}}{}_i$ is output in dimensionless units – fractions of gravitational acceleration g. The non-orthogonality matrix quantifies the influence of acceleration along the reference axes j and k on the considered axis i, where, for a tri-axial accelerometer, $i,j,k \in \{x,y,z\}$. In this article it is assumed that random error ε_i is caused only by electronic noise in the output signal.

For a tri-axial accelerometer, eq. (1) can be rewritten in matrix form (random error excluded), which is more suitable for the purpose of calibration:

$$\underbrace{\begin{bmatrix} a_x^{\mathrm{m}} \\ a_y^{\mathrm{m}} \\ a_z^{\mathrm{m}} \end{bmatrix}}_{\mathbf{G}} = \underbrace{\begin{bmatrix} m_{xx} & m_{xy} & m_{xz} \\ m_{yz} & m_{yy} & m_{yz} \\ m_{zx} & m_{zy} & m_{zz} \end{bmatrix}}_{\mathbf{M}_0} \underbrace{\begin{bmatrix} a_x^{\mathrm{t}} \\ a_y^{\mathrm{t}} \\ a_z^{\mathrm{t}} \end{bmatrix}}_{\mathbf{A}} + \underbrace{\begin{bmatrix} B_x \\ B_y \\ B_z \end{bmatrix}}_{\mathbf{B}} \qquad (2)$$

where $m_{ii} = (1+S_i)$.

In the course of calibration are estimated elements of matrices $\mathbf{M}_0$ and $\mathbf{B}$. Then, eq. (2) may be rearranged to yield corrected results of measurement:

$$\underbrace{\begin{bmatrix} a_x^{\mathrm{c}} \\ a_y^{\mathrm{c}} \\ a_z^{\mathrm{c}} \end{bmatrix}}_{\mathbf{A_c}} = \underbrace{\begin{bmatrix} l_{xx} & l_{xy} & l_{xz} \\ l_{yx} & l_{yy} & l_{yz} \\ l_{zx} & l_{zy} & l_{zz} \end{bmatrix}}_{\mathbf{M}_0^{-1}} \underbrace{\begin{bmatrix} a_x^{\mathrm{m}} - B_x \\ a_y^{\mathrm{m}} - B_y \\ a_z^{\mathrm{m}} - B_z \end{bmatrix}}_{\mathbf{G}-\mathbf{B}} \qquad (3)$$

where l_{ij} are elements of the inverse of matrix $\mathbf{M}_0$ and $a^{\mathrm{c}}{}_i$ are the corrected results.

From eq. (3) measurement results for accelerometer axes x and z can be written in expanded form:

$$a_x^{\mathrm{c}} = l_{xx}(a_x^{\mathrm{m}} - B_x) + l_{xy}(a_y^{\mathrm{m}} - B_y) + l_{xz}(a_z^{\mathrm{m}} - B_z) \qquad (4)$$

$$a_z^{\mathrm{c}} = l_{zx}(a_x^{\mathrm{m}} - B_x) + l_{zy}(a_y^{\mathrm{m}} - B_y) + l_{zz}(a_z^{\mathrm{m}} - B_z) \qquad (5)$$

External sources of uncertainty (fig. 8), independent of the instrument itself, include: acceleration disturbances both along and off the sensor reference axis, misalignment of sensor reference axis and the measurand direction, and fluctuations of environment temperature.

The temperature influence will not be considered in this paper, because of short duration of the measurement in the experiment, so temperature effects are negligible.

Systematic effects associated with misalignment of X_{W} axis of inertial frame (direction of the measurand) and x_{A} reference axis of the sensor, as well as with disturbance accelerations, are considered with aid of fig. 9.

Disturbance accelerations in the present experiment include (always present) acceleration of gravity and the acceleration caused by unevenness of the ground. For simplicity both accelerations were assumed to have vertical direction and their net effect is denoted $a_Z\mathbf{e}_{z\mathrm{W}}$, marked as thick red vector in fig. 9. This assumption can be satisfied in laboratory conditions.

In fig. 9, in contrast to fig. 7, axes of coordinate systems $O_{\mathrm{A}}x_{\mathrm{A}}z_{\mathrm{A}}$ and $O_{\mathrm{R}}x_{\mathrm{R}}z_{\mathrm{R}}$ do not coincide, but are rotated with respect to each other through angle κ. This angle accounts for constant misalignment between sensor reference axes and the vehicle reference axes introduced during mounting.

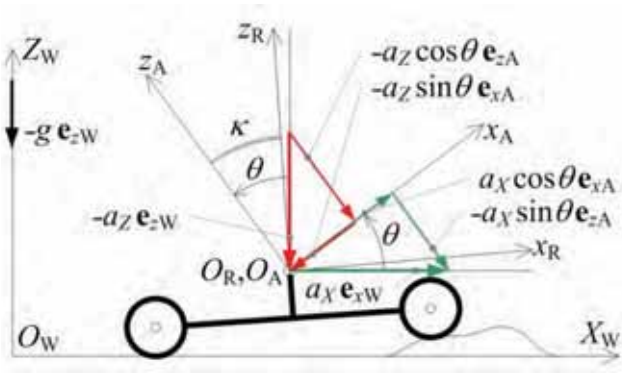

Fig. 9. Error of acceleration a_X due to variable misalignment of accelerometer's x_{A} axis and measurand direction X_{W}, and due to disturbance acceleration a_Z

Rys. 9. Błąd przyspieszenia a_X spowodowany zmianą niewspółosiowości kierunku mezurandu X_{W} i osi x_{A} akcelerometru, oraz przyspieszeniem zakłócającym a_Z

In fig. 9 robot's pitch angle (Tait-Bryan convention of Euler angles) about y_{R} axis is described with directed angle θ between Z_{W} axis of the inertial system and z_{A} axis of accelerometer. Unlike the constant angle κ, the angle θ may vary during vehicle movement, because of uneven ground surface.

Equations derived below are a valid model of reality, if the following conditions are satisfied: (1) robot body does not tilt to the side (i.e., motion takes place in plane of fig. 9) and (2) the angles θ and κ are small angles (i.e. smaller than 5°). These assumptions can be satisfied to a large extent in laboratory conditions, providing that horizontal and even surface is chosen for experiments.

From fig. 9 directly follow the expressions for accelerations along x_{A} and z_{A} accelerometer axes generated by acceleration of interest a_X and disturbance acceleration a_Z:

$$a_{xA} = a_X\cos\theta - a_Z\sin\theta\,, \qquad (6)$$

$$a_{zA} = -a_X\sin\theta - a_Z\cos\theta\,. \qquad (7)$$

After taking into account the assumption about small angles, equations (6) and (7) can be simplified to:

$$a_{xA} = a_X - a_Z\theta\,, \qquad (8)$$

$$a_{zA} = -a_X\theta - a_Z\,. \qquad (9)$$

Hence, accelerations a_X and a_Z can be determined as:

$$a_X = a_{xA} + a_Z\theta\,, \qquad (10)$$

$$a_Z = -a_{zA} - a_X\theta\,, \qquad (11)$$

and inserting eq. (11) into (10) yields

$$a_X = a_{xA} - a_{zA}\theta - a_X\theta^2 . \tag{12}$$

If one assumes that $\theta^2 \cong 0$, which is reasonable for $\theta < 5^{\circ}$, then one may eventually write

$$a_X = a_{xA} - a_{zA}\theta . \tag{13}$$

After making use of equations (4) and (5), accelerations along accelerometer reference axes x_A and z_A can be substituted with values of corrected measurement results a^c_x and a^c_z

$$a'_X = a^c_x - a^c_z\theta . \tag{14}$$

where a'_X is expressed in fractions of gravitational acceleration g. One may obtain the acceleration a_X (i.e., in SI units) by performing multiplication of equation (14) by the value of gravitational acceleration g present at the site of calibration

$$a_X = a'_X g = (a^c_x - a^c_z\theta)g . \tag{15}$$

The angle θ in equation (15), for the needs of the present work, is expressed in the following way

$$\theta = \kappa + \alpha_0 + \alpha - \alpha_0 \tag{16}$$

where: α is the angle between robot z_R axis and the vertical, and α_0 is initial value of this angle (i.e., before the motion begins).

If one sets

$$\theta_0 = \kappa + \alpha_0 \tag{17}$$

and

$$\delta\alpha = \alpha - \alpha_0, \tag{18}$$

then eq. (16) becomes

$$\theta = \theta_0 + \delta\alpha. \tag{19}$$

The reason for expressing angle θ in the form of (19) is that measurement of angle θ_0 can be done by means of an accelerometer, with method described in [14]. However, that method is valid when accelerometer is subjected to only acceleration of gravity, and not to acceleration from motion. In the present experiment the angle $\delta\alpha$ is not measured during motion, because of technical limitations and introduces some uncertainty to the result.

Expression for the angle θ_0 was chosen as:

$$\theta_0 = \arctan\frac{a^c_{x,0}}{a^c_{z,0}} , \tag{20}$$

where index "0" at a quantity means that its value should be obtained when the robot does not move. During each experiment there is a period of measurement of quantities a^c_x and a^c_z lasting for several seconds before robot's motion begins, and those data are used to determine the angle θ_0.

The formula (20) was chosen based on considerations of work [14] concerning minimization of uncertainty, with additional assumption introduced here that tilt angle is equal to robot's pitch angle (roll angle is assumed 0).

Velocity change Δv_X due to time-variable acceleration $a_X(t)$ over time interval $t \in \langle t_0, t_1 \rangle$ is given by

$$\Delta v_X \Big|_{t_0}^{t_1} = v_X(t_1) - v_X(t_0) = \int_{t_0}^{t_1} a_X(t)dt . \tag{21}$$

After passing to numerical form of the integral (21) one gets

$$\Delta v_X \Big|_{t_0}^{t_1} = v_X(t_1) - v_X(t_0) = \sum_{n=\mathrm{n}(t_0)}^{\mathrm{n}(t_1)} a_X(t_n)\Delta t_n , \tag{22}$$

where: $\mathrm{n}(t)$ is certain function which maps continuous time t to its discrete counterpart t_n, the step time of integration is $\Delta t_n = t_{n+1} - t_n$, and subscript n at a quantity denotes sample number in the discrete signal which corresponds to time t_n.

From now on, to make the notation more concise, the value of a time-variable quantity at the discrete time instant t_n will be denoted only with the subscript n (e.g., $a_X(t_n) \Rightarrow a_{X,n}$).

In this article $Dv_{X,n}$ denotes the change of velocity v_X at a single integration step Δt_n (i.e., small change of velocity v_X) which is equal to

$$Dv_{X,n} = \Delta v_X \Big|_{t_n}^{t_{n+1}} = a_{X,n}\Delta t_n . \tag{23}$$

After taking into account eq. (15) in (23) one gets

$$Dv_{X,n} = (a^c_{x,n} - a^c_{z,n} \times \theta_n) \times g \times \Delta t_n . \tag{24}$$

As suggested by the document [15], the *uncertainty* of a measurand y determined from other quantities can be calculated according to the following formula:

$$u_c^2(y) = \sum_{i=1}^{N}\left(\frac{\partial \mathrm{f}}{\partial q_i}\right)^2 u^2(q_i) = \sum_{i=1}^{N} u_i^2(y) \tag{25}$$

where: $u_c(y)$ is the combined standard uncertainty of a measurand y, f is a function describing the measurand y in terms of input quantities q_i and $u(q_i)$ is the standard uncertainty of q_i.

The combined standard uncertainties of quantities $a^c_{x,n}$ and $a^c_{z,n}$ are calculated based on eq. (4) and eq. (5):

$$\begin{aligned} u_c(a^c_{x,n}) = \Big[&\big((a^{\mathrm{m}}_{x,n} - B_x)u(l_{xx})\big)^2 + \big((a^{\mathrm{m}}_{y,n} - B_y)u(l_{xy})\big)^2 + \\ &+ \big((a^{\mathrm{m}}_{z,n} - B_z)u(l_{xz})\big)^2 + \big(l_{xx}u(a^{\mathrm{m}}_{x,n})\big)^2 + \big(l_{xy}u(a^{\mathrm{m}}_{y,n})\big)^2 + \\ &+ \big(l_{xz}u(a^{\mathrm{m}}_{z,n})\big)^2 + \big(-l_{xx}u(B_x)\big)^2 + \big(-l_{xy}u(B_y)\big)^2 + \\ &+ \big(-l_{xz}u(B_z)\big)^2\Big]^{\frac{1}{2}} \end{aligned} \tag{26}$$

$$\begin{aligned} u_c(a^c_{z,n}) = \Big[&\big((a^{\mathrm{m}}_{x,n} - B_x)u(l_{zx})\big)^2 + \big((a^{\mathrm{m}}_{y,n} - B_y)u(l_{zy})\big)^2 + \\ &+ \big((a^{\mathrm{m}}_{z,n} - B_z)u(l_{zz})\big)^2 + \big(l_{zx}u(a^{\mathrm{m}}_{x,n})\big)^2 + \big(l_{zy}u(a^{\mathrm{m}}_{y,n})\big)^2 + \\ &+ \big(l_{zz}u(a^{\mathrm{m}}_{z,n})\big)^2 + \big(-l_{zx}u(B_x)\big)^2 + \big(-l_{zy}u(B_y)\big)^2 + \\ &+ \big(-l_{zz}u(B_z)\big)^2\Big]^{\frac{1}{2}} \end{aligned} \tag{27}$$

Based on eq. (19) and eq. (20) the uncertainty of quantity θ_n can be written as

$$\begin{aligned} u_c(\theta_n) = \Bigg[&u^2(\delta\alpha_n) + \left(\frac{a^c_{z,0}}{\left(a^c_{z,0}\right)^2 + \left(a^c_{x,0}\right)^2}u\left(a^c_{x,0}\right)\right)^2 + \\ &+ \left(-\frac{a^c_{x,0}}{\left(a^c_{z,0}\right)^2 + \left(a^c_{x,0}\right)^2}u\left(a^c_{x,0}\right)\right)^2\Bigg]^{\frac{1}{2}} . \end{aligned} \tag{28}$$

Finally, based on eq. (24), the uncertainty of quantity $Dv_{X,n}$ is given by

$$u_c(Dv_{X,n}) = \Big[\big(g\Delta t_n u(a^c_{x,n})\big)^2 + \big(-\theta_n g\Delta t_n u(a^c_{z,n})\big)^2 + \\ + \big(-a^c_{z,n} g\Delta t_n u(\theta_n)\big)^2 + \big((a^c_{x,n} - a^c_{z,n}\times\theta_n)\Delta t_n u(g)\big)^2 + \\ + \big((a^c_{x,n} - a^c_{z,n}\times\theta_n) g u(\Delta t_n)\big)^2\Big]^{\frac{1}{2}} \quad . \qquad (29)$$

Equation (29) describes the uncertainty of the small change of velocity at a single time interval Δt_n. On the other hand, the formula to describe the uncertainty of measurement of velocity in time interval $t\in <t_b, t_e>$ reads

$$u_c(v_{X,N}) = \sqrt{\sum_{n=1}^{N} u_c^2(Dv_{X,n})} \qquad (30)$$

where $n(t_b) = 1$ and $n(t_e) = N$ (see comment at eq. (22)), and it is assumed that the measurement begins at time instant t_b with initial velocity $v_{X,0} = 0$ and initial uncertainty $u_c(v_{X,0}) = 0$.

In the case when velocity measurements are repeated in unchanged conditions, the best estimate of velocity is obtained by averaging velocities from individual measurements $v_{X,n}$ at each discrete time t_n (assumed $v_{X,0} = 0$ in eq. (22)). One component of uncertainty of this average velocity can be evaluated using type A procedure (the procedure described in [15]), and the other component, associated with systematic effects, is calculated on the basis of eq. (29) with condition that uncertainties of instrument's raw results due to random errors (noise), e.g. $u(a^m_x)$, are set to 0.

The uncertainty of velocity measurement in time interval $t\in <t_b, t_e>$ for repeated measurements is

$$u_c(\bar{v}_{X,N}) = \sqrt{\sum_{n=1}^{N} \hat{u}_c^2(Dv_{X,n}) + s^2(\bar{v}_{X,N})} \qquad (31)$$

where: $\hat{u}_c(Dv_{X,n})$ is uncertainty calculated from formula (29), but involving component uncertainties such that uncertainties of instrument's indications, e.g. $u(a^m_x)$, are all set to 0, and $s(\bar{v}_{X,N})$ is obtained from formula

$$s^2(\bar{v}_{X,N}) = \frac{s^2(v_{X,N})}{M} \qquad (32)$$

where: $s(v_{X,N})$ is the standard deviation of values of velocity in the sample consisting of all repeated measurements for the time instant t_N, and M is the number of repeated measurements.

5. Results

The experiment with mobile robot, described in Section 3, has been repeated $M = 12$ times. Accelerometers A1 and A2 were simultaneously mounted on the robot.

Fig. 10 (a) shows M velocities v_X of the mobile platform (dark lines), determined according to the measurement model described in the previous Section on the basis of accelerometer A1 indications, as well as their average $\bar{v}_X$ (bright line).

Fig. 10 (b) shows the average velocity $\bar{v}_X$ of mobile platform (continuous line), compared with reference velocity from wheel encoder (dashed line).

In case of the average velocity $\bar{v}_X$, in fig. 10 (b), there is also shown its standard uncertainty $u_c(\bar{v}_{X,N})$. It should be emphasized that uncertainty of velocity at time instant t_n takes into account uncertainties at preceding time instants according to equation (31). In this way the shown uncertainty is accumulative, and grows with elapsed time of measurement.

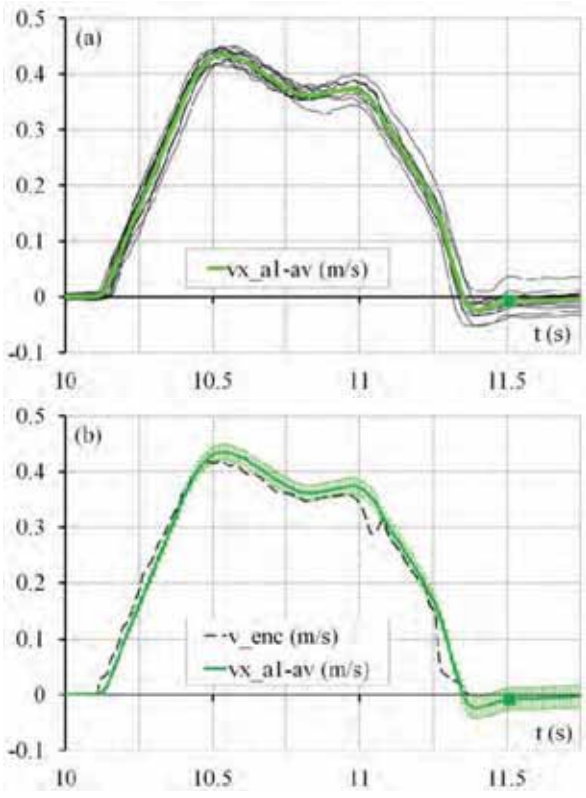

Fig. 10. Accelerometer A1: time courses of M = 12 velocities v_X of the mobile robot (dark lines) and their average (bright line) (a), the average velocity with its standard uncertainty (continuous line with bright "corridor") and reference velocity (dashed line) (b)

Rys. 10. Akcelerometr A1: przebiegi czasowe M = 12 prędkości v_X robota mobilnego (linie ciemne) oraz ich średnia (linia jasna) (a), średnia prędkość z niepewnością standardową (linia ciągła z jasnym „korytarzem") i prędkość odniesienia (linia przerywana) (b)

Apart from random influences, the presented standard uncertainty also takes into account uncertainty associated with systematic effects, e.g. uncertainty of corrections obtained from calibration.

The corrections seem not very accurate, because in the portion of the graph between 10.5 s and 11 s velocity $\bar{v}_X$ obtained from acceleration sensor A1 is noticeably greater than the reference velocity from encoders v_{enc}.

Just before 11.5 s, there is a drop of velocity below 0, which suggests robot moving backwards. This might have been caused by the backward swing of centre of mass just after the robot finished braking (this effect is known to users of e.g. passenger cars). It would be possible to verify this hypothesis, if the value of θ angle were available during motion.

Results for acceleration sensor A2 shown in fig. 11 are qualitatively similar to those for acceleration sensor A1.

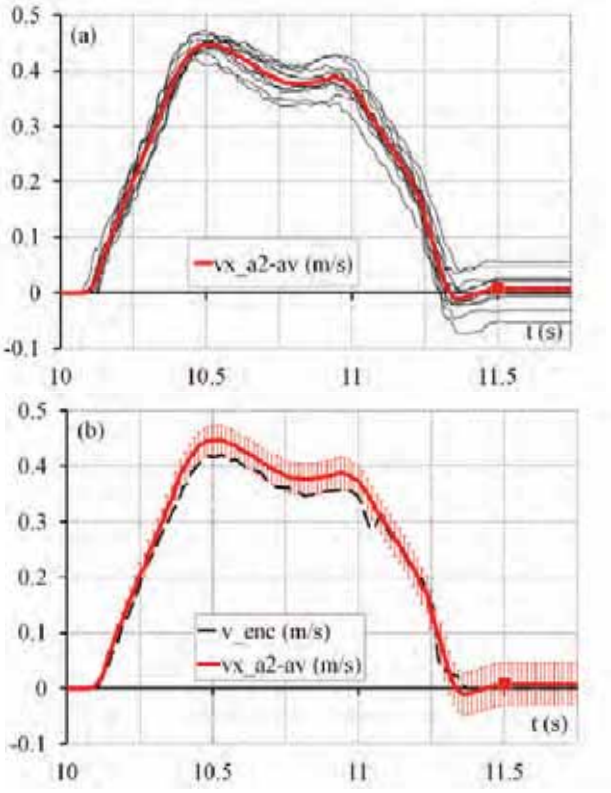

Fig. 11. Accelerometer A2: time courses of M = 12 velocities v_X of the mobile robot (dark lines) and their average (bright line) (a), the average velocity with its standard uncertainty (continuous line with bright "corridor") and reference velocity (dashed line) (b)

Rys. 11. Akcelerometr A2: przebiegi czasowe M = 12 prędkości v_X robota mobilnego (linie ciemne) oraz ich średnia (linia jasna) (a), średnia prędkość z niepewnością standardową (linia ciągła z jasnym „korytarzem") i prędkość odniesienia (linia przerywana) (b)

Tab. 2. Parameters of time-courses of velocities obtained from accelerometers A1 and A2; parameters pertain to time instant t_n = 11.5 s

Tab. 2. Parametry przebiegów czasowych prędkości uzyskanych z akcelerometrów A1 i A2; parametry dotyczą chwili czasowej t_n = 11,5 s

	A1	A2
Error[1)] of v_X after 1.5 s (m/s)	0.04	0.06
Error of $\overline{v}_X$ after 1.5 s (m/s)	-0.01	0.01
$u_c(\overline{v}_{X,N})$ after 1.5 s (m/s)	0.02	0.04
$s(v_{X,N})$ at 1.5 s (m/s)	0.006	0.009

[1)] Maximum error from all individual measurements

In tab. 2 is shown a comparison of parameters of the time-courses of velocities at the chosen time instant t_n =11.5 s (marked on figures 10 and 11 with the bold square).

Data in tab. 2 substantiate visual impression that velocity measured by means of A1 has smaller standard deviation and smaller uncertainty in comparison to A2. Similarly, maximum error from individual errors of all measurements is larger for the sensor A2. It is worth pointing out that by averaging 12 signals, error could be reduced by more than 75 % in comparison to the worst individual measurement obtained.

Tab. 3. Data necessary to calculate uncertainty of v_X for the accelerometer A1

Tab. 3. Dane do obliczenia niepewności v_X dla akcelerometru A1

(1)	(2)	(3)	(4)	(5)	(6)
i	q_i	est(q_i)	$u(q_i)$	Eq.	$u_i^2(y)$
1	l_{xx} (–)	0.98	1.0×10^{-3}	(4)	3.3×10^{-9}
2	l_{xy} (–)	0.008	2.7×10^{-3}	(4)	1.4×10^{-8}
3	l_{xz} (–)	–0.019	2.0×10^{-3}	(4)	3.8×10^{-6}
4	$a^{\mathrm{m}}{}_x$ (–)	0.01	3.8×10^{-3}	(4)	1.4×10^{-5}
5	$a^{\mathrm{m}}{}_y$ (–)	–0.027	3.0×10^{-3}	(4)	5.8×10^{-10}
6	$a^{\mathrm{m}}{}_z$ (–)	0.833	4.9×10^{-3}	(4)	8.5×10^{-9}
7	B_x (–)	0.047	3.6×10^{-3}	(4)	1.2×10^{-5}
8	B_y (–)	–0.018	1.2×10^{-3}	(4)	9.4×10^{-11}
9	B_z (–)	–0.146	7.5×10^{-3}	(4)	2.0×10^{-8}
10	l_{zx} (–)	–0.004	1.6×10^{-2}	(5)	8.4×10^{-7}
11	l_{zy} (–)	0.004	1.8×10^{-3}	(5)	6.4×10^{-9}
12	l_{zz} (–)	1.008	1.3×10^{-3}	(5)	1.5×10^{-6}
13	$a^{\mathrm{m}}{}_x$ (–)	0.01	3.8×10^{-3}	(5)	2.2×10^{-10}
14	$a^{\mathrm{m}}{}_y$ (–)	–0.027	3.0×10^{-3}	(5)	1.4×10^{-10}
15	$a^{\mathrm{m}}{}_z$ (–)	0.833	4.9×10^{-3}	(5)	2.4×10^{-5}
16	B_x (–)	0.047	3.6×10^{-3}	(5)	1.9×10^{-10}
17	B_y (–)	–0.018	1.2×10^{-3}	(5)	2.3×10^{-11}
18	B_z (–)	–0.146	7.5×10^{-3}	(5)	5.7×10^{-5}
19	$\delta\alpha$ (rad)	0	1.8×10^{-3}	(19)	3.1×10^{-6}
20	$a^{c}{}_{x,0}$ (–)	–0.132	5.5×10^{-3}	(19)	3.0×10^{-5}
21	$a^{c}{}_{z,0}$ (–)	0.985	9.3×10^{-3}	(19)	1.5×10^{-6}
22	$a^{c}{}_x$ (–)	–0.074	5.5×10^{-3}	(24)	2.9×10^{-7}
23	$a^{c}{}_z$ (–)	0.988	9.2×10^{-3}	(24)	1.5×10^{-8}
24	θ (rad)	–0.133	5.9×10^{-3}	(24)	3.3×10^{-7}
25	g(m/s^2)	9.81213	3.0×10^{-6}	(24)	3.0×10^{-18}
26	Δt (s)	0.01	1.6×10^{-3}	(24)	8.1×10^{-7}

Despite the fact that measurement duration was short, the uncertainty associated with obtained velocity is significant. In order to highlight the most important sources of uncertainty, an appropriate analysis has been carried out.

Component variances (i.e., standard uncertainty squared) necessary to calculate the combined uncertainty

of velocity change at a single time step $u_c(Dv_{X,n})$ are gathered in the column 6 of tab. 3 (A1) and tab. 4 (A2). The tables also contain all data necessary to calculate the uncertainty components $u_i(y)$ (notation as in eq. (25)), that is, estimates of values of quantities q_i (col. 3), uncertainties of those estimates (col. 4) and the number of equation on which was based calculation of the sensitivity coefficient for the given uncertainty component (col. 5).

Tab. 4. Data necessary to calculate uncertainty of v_X for the accelerometer A2

Tab. 4. Dane do obliczenia niepewności v_X dla akcelerometru A2

(1)	(2)	(3)	(4)	(5)	(6)
i	q_i	est(q_i)	$u(q_i)$	Eq.	$u_i^2(y)$
1	l_{xx} (–)	1.061	5.0×10^{-3}	(4)	3.2×10^{-8}
2	l_{xy} (–)	–0.001	6.2×10^{-3}	(4)	4.7×10^{-9}
3	l_{xz} (–)	–0.0011	1.0×10^{-4}	(4)	1.0×10^{-8}
4	$a^{m}{}_{x}$ (–)	–0.103	1.7×10^{-3}	(4)	3.3×10^{-6}
5	$a^{m}{}_{y}$ (–)	0.036	1.8×10^{-3}	(4)	1.3×10^{-12}
6	$a^{m}{}_{z}$ (–)	–0.558	2.8×10^{-3}	(4)	1.0×10^{-11}
7	B_x (–)	0.067	5.0×10^{-3}	(4)	2.8×10^{-5}
8	B_y (–)	–0.025	5.0×10^{-3}	(4)	1.0×10^{-11}
9	B_z (–)	–0.448	2.6×10^{-3}	(4)	8.7×10^{-12}
10	l_{zx} (–)	–0.006	7.6×10^{-3}	(5)	7.4×10^{-8}
11	l_{zy} (–)	–0.015	7.6×10^{-3}	(5)	7.0×10^{-9}
12	l_{zz} (–)	0.991	5.3×10^{-3}	(5)	2.9×10^{-5}
13	$a^{m}{}_{x}$ (–)	–0.103	1.7×10^{-3}	(5)	1.0×10^{-10}
14	$a^{m}{}_{y}$ (–)	0.036	1.8×10^{-3}	(5)	7.1×10^{-10}
15	$a^{m}{}_{z}$ (–)	–0.558	2.8×10^{-3}	(5)	7.7×10^{-6}
16	B_x (–)	0.068	5.0×10^{-3}	(5)	8.8×10^{-10}
17	B_y (–)	–0.025	5.0×10^{-3}	(5)	5.5×10^{-9}
18	B_z (–)	–0.449	2.6×10^{-3}	(5)	6.6×10^{-6}
19	$\delta\alpha$ (rad)	0	1.8×10^{-3}	(19)	3.1×10^{-6}
20	$a^{c}{}_{x,0}$ (–)	–0.007	5.6×10^{-3}	(19)	3.2×10^{-5}
21	$a^{c}{}_{z,0}$ (–)	1.001	6.6×10^{-3}	(19)	1.9×10^{-9}
22	$a^{c}{}_{x}$ (–)	0.037	5.6×10^{-3}	(24)	7.4×10^{-7}
23	$a^{c}{}_{z}$ (–)	0.998	6.6×10^{-3}	(24)	4.4×10^{-11}
24	θ (rad)	–0.007	5.9×10^{-3}	(24)	8.1×10^{-7}
25	g (m/s^2)	9.81213	3.0×10^{-6}	(24)	4.2×10^{-18}
26	Δt (s)	0.016	4.0×10^{-3}	(24)	2.9×10^{-6}

Values of sensitivity coefficients necessary to calculate uncertainty components $u_i(y)$ were obtained for estimates of q_i calculated as an average of attained values within time interval $t \in \langle t_b, t_e \rangle$ when robot was in motion. That procedure was followed, because as values of q_i change during motion, values of sensitivity coefficients change accordingly, and they influence uncertainty components $u_i(y)$. Averaging over time interval of robot motion was performed to get representative estimates of the involved quantities necessary for the subsequent analysis.

Data for calibration were obtained from the 6 position static test and the elements of matrix $\mathbf{M}_0$ (eq. (2)) were found with the method of least squares. Those values are constant during motion. Standard uncertainties of quantities 2–3, 7–9, 10–12 and 16–18 (numbers i in col. (1)) were calculated according to the type A procedure from repeated calibrations (2 repetitions).

Standard uncertainty of quantity 1, that is, of the element l_{xx} of the matrix $\mathbf{M}_0^{-1}$, was obtained from formula

$$u(l_{xx}) = \sqrt{u_{\text{cal}}^2(l_{xx}) + (\max(e_{\text{lin}}(m_{xx}))/\sqrt{3})^2} \qquad (34)$$

where u_{cal} is component of $u(l_{xx})$ due to inaccuracy of calibration, and e_{lin} is error of nonlinearity of accelerometer scale factor (with assumed rectangular distribution) based on results provided below.

Results of dynamic test of accelerometers described in Section 3 are shown in fig. 12. Presented data are averaged results from 10 series. Each data point represents the amplitude of x-axis acceleration signal measured by the instrument subjected to harmonic kinematic excitation.

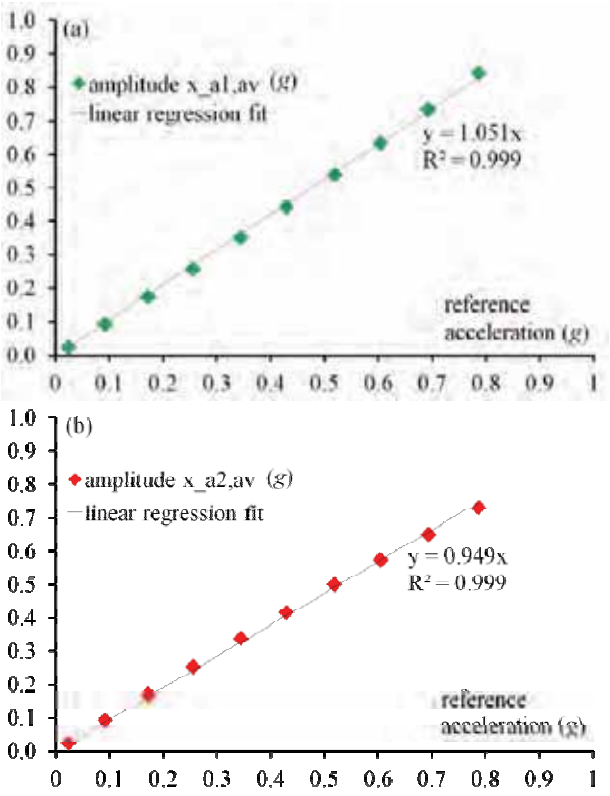

Fig. 12. Measured vs. reference acceleration for accelerometers A1 (a) and A2 (b)

Rys. 12. Zależność między przyspieszeniem odniesienia i zmierzonym dla akcelerometru A1 (a) oraz A2 (b)

In case of both instruments, error of nonlinearity of scale factor can be observed, which for the presented regression fit lines is at the level of 1000 ppm FS (parts per million of Full Scale) for accelerometer A1, and 5000 ppm FS for A2. Those values qualify the investigated sensors into

the low performance segment of the map of accelerometers' applications [4].

Values of quantities a^{m}_{x}, a^{m}_{y}, a^{m}_{z} vary during motion. For this reason as the estimates are provided average values attained during the motion phase. Uncertainties 4–6 and 13–15 were evaluated according to the type A procedure. Those uncertainties reflect noise present in the output for given instrument axis. Number of samples taken into account was 1000 in case of A1 and 500 in case of A2. It is assumed that electronic noise does not depend on measurement conditions, so this value is the same whether the robot is stationary or in motion.

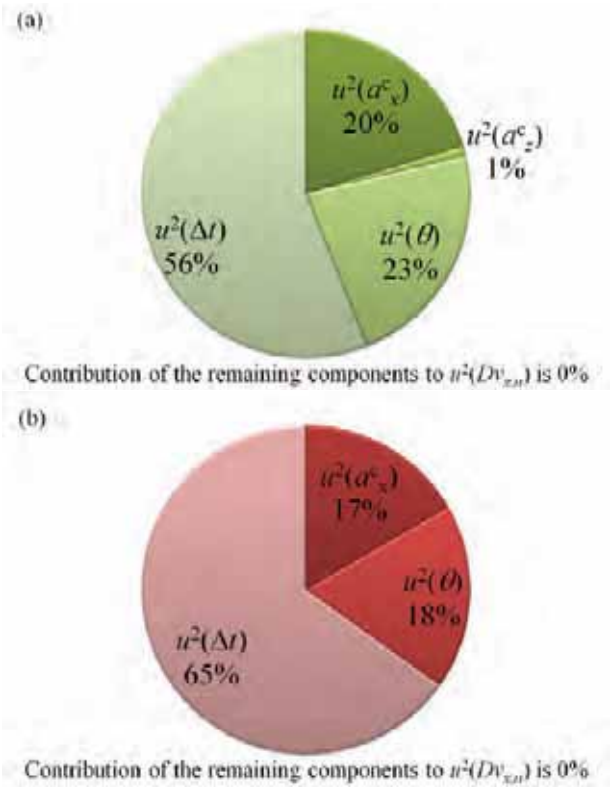

Fig. 13. Breakdown of uncertainty of velocity Dv_X: for A1 based on tab. 3 (a), for A2 based on tab. 4 (b)

Rys. 13. Udział składowych niepewności prędkości Dv_X: dla A1 na podst. tab. 3 (a), dla A2 na podst. tab. 4 (b)

Even though the experimental floor was carefully selected to have even and horizontal surface, angle θ might have varied slightly. However, during the experiment the value of actual θ angle was not measured – deviation $\delta\alpha$ of the actual θ angle from its initial value θ_0 was assumed 0 rad, and inaccuracy of this assumption was included into uncertainty. Uncertainty 19 was evaluated from the type B procedure based on available data characterising the ground. It was estimated that for 67 % of measurement time $\delta\alpha$ will change by no more than ±0.1 degree, that is one axle of the robot will rise or fall with respect to another by no more than 1 mm, and distribution is normal with mean of 0 degrees.

Values of corrected accelerations 20 and 21 for determination of the initial angle θ_0 were obtained based on the average from raw indications a^{m}_{x}, a^{m}_{y}, a^{m}_{z} (not included in tables) gathered in the initial phase, preceding motion of the robot, of duration of nearly 10 s (A1: 1000 samples, A2: 600 samples), and on necessary data from tab. 3 or tab. 4. Uncertainties were calculated from equations (26) and (27).

Value of gravitational acceleration was obtained for the gravitation measurement station Józefosław (site code: JOZE) [16] which is situated close to the site of calibration. Uncertainty 25 was evaluated from the type B procedure, as it was the value of resolution of instrument given in the source [16].

Value of Δt was estimated based on data from several individual series of measurements – 10 000 samples in total. Value of Δt has nominal value stated by the accelerometer's manufacturer. In case of A1 it was 10 ms, and in case of A2, 16.667 ms (60 samples/s). Uncertainty 26 was evaluated from the type A procedure from the same data as the average value.

Estimates of values of quantities 22–24 were calculated based on equations (4), (5) and (19) using necessary data from tab. 3 (tab. 4). Corresponding uncertainties were calculated based on equations (26), (27) and (28).

In the pie charts in fig. 13, data are taken from tab. 3 and 4 to illustrate contributions to the combined variance of small velocity change during single time step $Dv_{X,n}$ for the two examined accelerometers (eq. (29)).

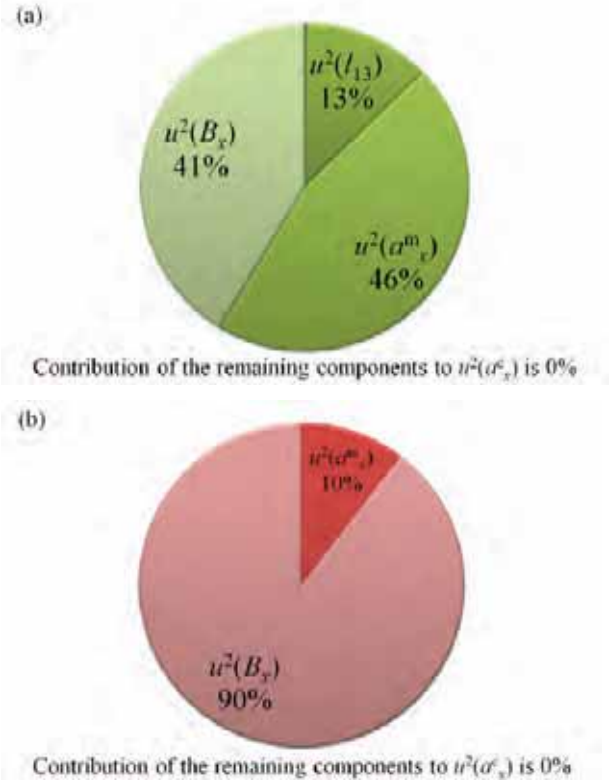

Fig. 14. Breakdown of uncertainty of acceleration a^c_x: for A1 based on tab. 3 (a), for A2 based on tab. 4 (b)

Rys. 14. Udział składowych niepewności przyspieszenia a^c_x: dla A1 na podst. tab. 3 (a), dla A2 na podst. tab. 4 (b)

For both instruments the largest source of uncertainty is the uncertainty of time interval between successive samples of acceleration Δt_n. The actual error of Δt_n

will vary in random fashion from sample to sample, so it can be mitigated by averaging results of repeated measurements, because expected value of the random error is 0. If the measurements cannot be repeated, as is the case, for instance, in navigation applications, then this uncertainty source seems to be critical to the overall accuracy of velocity measurement. As far as measurement nodes are concerned, this uncertainty may be influenced by accuracy of the node internal oscillator (which governs time interval at which data are sent from the node to acquisition system), bus errors, delays on the side of the computer operating system, etc.

Two other important sources of uncertainty of $Dv_{X,n}$ are: uncertainty associated with value of the angle θ, and uncertainty of value of the corrected acceleration a^c_x.

The uncertainty of measurement of angle θ, according to the presented model, possesses components associated with initial constant angle θ_0 and with variable angle during motion $\delta\alpha$.

Uncertainty of the initial angle θ_0 critically depends on inaccuracy of instrument's corrections. Uncertainty of the variable part may be reduced by introducing measurement of angle $\delta\alpha$ during motion.

The uncertainty of the corrected acceleration a^c_x contributes about 20 % to the total uncertainty of $Dv_{X,n}$.

In fig. 14 are visualised contributions to the combined uncertainty of a^c_x for each sensor.

It is evident, that there are two major sources of uncertainty of quantity a^c_x: (1) uncertainty of corrections from calibration and (2) noise in the raw indication a^m_x from sensitive axis x of the sensor.

Noise is a random error, and, as mentioned earlier in discussion of uncertainty of Δt, it can be mitigated by averaging results from multiple measurements in repeatable conditions. On the other hand, if repeated measurements are not possible, then axis noise becomes an important property of the accelerometer which may influence the measurement of velocity in significant way (on condition that high quality calibration has been performed). The importance of sensor noise has been long recognized by navigation industry: the better is the performance of the instrument in terms of noise, the higher is the price.

6. Conclusion

The objective of the present study was to assess the uncertainty of measurement of velocity of a vehicle by means of recently produced budget MEMS accelerometers from perspective of using the measurement results for validation of a non-linear dynamics model of unmanned ground vehicle.

In order to achieve the stated goal, model of measurement has been developed with accompanying uncertainties following guidance of document [15]. Calibration of the instruments, tests for non-linearity and experimental measurements of velocity of an UGV have been carried out.

It has been found that in the present experiment standard uncertainty of velocity determined on the basis of measurement of acceleration was of the order of 0.02–0.04 m/s after 1.5 s of measurement duration.

This level of uncertainty was considered not satisfying, and sources which contribute to the uncertainty of velocity have been analysed. The uncertainty is most influenced by: (1) inaccuracy of time basis for measured acceleration, (2) inaccuracy of calibration procedure, (3) electronic noise at the instrument output and (4) inaccuracy of measurement of variable angle θ between accelerometer's reference axis z_A and the vertical direction.

In the applications where measurements can be repeated many times in unchanged conditions, the most important sources of uncertainty are (2) and (4), because uncertainties (1) and (3) can be significantly reduced by averaging the results.

In view of that, it is concluded that – for the purpose of characterisation of motion of unmanned ground vehicles in typical terrains of operation – low-cost acceleration sensors can be used with the described method of velocity measurement, on conditions that high quality of calibration procedure and measurement of θ are guaranteed. To satisfy those conditions will be the objective of author's future work.

Acknowledgements

Author wishes to thank Mr. Krzysztof Trzcinka for making available the Tira-VIB facility and Mr. Andrzej Bratek for help with establishing communications through CAN protocol. Both sirs work in OUP/PIAP.

The work has been realised as a part of the project entitled "Dynamics modeling of four-wheeled mobile robot and tracking control of its motion with limitation of wheels slip". The project is financed from the means of the National Science Centre of Republic of Poland granted on the basis of decision number DEC-2011/03/B/ST7/02532.

Bibliography

1. Ray L.R., Brande D.C., Lever J.H., *Estimation of net traction for differential-steered wheeled robots*, "Journal of Terramechanics", 46/2009, 75–87.
2. Trojnacki M., *Modeling and Motion Simulation of a Three-Wheeled Mobile Robot with Front Wheel Driven and Steered Taking into Account Wheels' Slip*, "Archive of Applied Mechanics", 5/2012, [DOI 10.1007/s00419-012-0636-2].
3. Marinis T.F., *The future of Microelectromechanical systems (MEMS)*, "Strain", 45/2009, 208–220.
4. Barbour N., Schmidt G., *Inertial sensor technology trends*, "IEEE Sensors Journal", Vol. 1, No. 4, 2001, 332–339.
5. Pang G., Liu H., *Evaluation of a Low-cost MEMS Accelerometer for Distance Measurement*, "Journal of Intelligent and Robotic Systems", 30/2001, 249–265.
6. Onodera R., Mimura N., Shishido M., *An efficient calibration method for a novel 6-DOF acceleration sensor system and application to measurement of a vehicle motion*, "Proceedings of IEEE Sensors Conf.", art. no. 5690441, 2010, 600–605.

7. [www.analog.com] – Analog Devices (7 Dec 2012).
8. [www.mikrosensor.de] – Micro-Sensor GmbH (7 Dec 2012).
9. [www.phidgets.com] – Phidgets Inc. – Unique and Easy to Use USB Interfaces (7 Dec 2012).
10. [www.analog.com/en/mems-sensors/mems-inertial-sensors/adxl330/products/product.html] – Analog Devices (7 Dec 2012).
11. [www.antyterroryzm.com/product/en/scout] – PIAP Scout mobile robot (7 Dec 2012).
12. Syed Z.F., Aggarwal P., Goodall C., Niu X., El-Sheimy N., *A new multi-position calibration method for MEMS inertial navigation systems*, "Meas. Sci. and Technol.", 18/2007, 1897–1907.
13. [www.peak-system.com] – Homepage of PEAK-System (7 Dec 2012).
14. Łuczak S., *Accelerometer-based measurements of axial tilt*, "Journal of Automation, Mobile Robotics & Intelligent Systems", Vol. 6, No. 1, 2012, 39–41.
15. Joint Committee for Guides in Metrology, *Evaluation of measurement data — Guide to the expression of uncertainty in measurement*, JCGM 100:2008, [www.bipm.org/en/publications/guides/gum.html].
16. [http://bgi.dtp.obs-mip.fr] – Absolute Gravity Database (7 Dec 2012).

Ewaluacja akcelerometrów MEMS pod kątem pomiaru prędkości pojazdów bezzałogowych

Streszczenie: W artykule poruszono problem pomiaru bezwładnościowego parametrów ruchu pojazdów. Celem pracy jest ocena niepewności pomiaru związanej z wyznaczaniem prędkości metodą całkowania przyspieszenia zmierzonego akcelerometrem typu MEMS. Dwa akcelerometry typu MEMS zostały poddane ocenie z punktu widzenia zastosowania charakteryzującego się krótkim czasem trwania pomiaru oraz możliwością jego powtarzania w niezmienionych warunkach. Zaprezentowano model matematyczny pomiaru prędkości wraz z towarzyszącą mu niepewnością. Akcelerometry zostały poddane procedurze kalibracji oraz wyznaczono nieliniowości dla ich współczynników skali dzięki wykorzystaniu urządzenia Tira-VIB do wygenerowania przyspieszeń o zmiennych wartościach. Czujniki zostały zamontowane na robocie kołowym, który wykonał w sposób powtarzalny manewr jazdy prostoliniowej na tej samej nawierzchni. Otrzymano niepewność standardową prędkości zmierzonej przy użyciu badanych akcelerometrów na poziomie 0,02–0,04 m/s dla przebiegu trwającego ok. 1,5 s, przy uśrednieniu danych z 12 przebiegów. Na podstawie wykonanej pracy można rekomendować tanie akcelerometry MEMS do pomiarów prędkości charakteryzujących się krótkim czasem trwania oraz możliwością powtarzania pomiarów. Należy zwrócić uwagę na minimalizację niepewności związanych z kalibracją instrumentów oraz pomiarem zmiennego kąta przechyłu pojazdu podczas ruchu.

Słowa kluczowe: akcelerometr MEMS, pomiar prędkości, niepewność pomiaru, dynamika pojazdów, pojazdy bezzałogowe

Przemysław Dąbek, MSc Eng.

He is a PhD student at the Chair of Vehicles and Fundamentals of Machine Design at the Lodz University of Technology, Poland. He holds the B.Eng. diploma from Coventry University, UK. Currently involved in research concerning identification of dynamics of small vehicles, with emphasis on tyre-road interaction, and their modelling for application in the Virtual Prototyping. Cooperates with the Industrial Research Institute for Automation and Measurements PIAP, Poland.

e-mail: pdabek@gmail.com